Quantitative optical imaging of the pharmacokinetics of fluorescent-specific antibodies to tumor markers through tissuelike turbid media

Israel Gannot*

Department of Biomedical Engineering, Faculty of Engineering, Tel Aviv University, Tel Aviv 69978, Israel, and National Institute of Child Health and Development, National Institutes of Health, Bethesda, Maryland 20892-5626

Avital Garashi

Department of Biomedical Engineering, Faculty of Engineering, Tel Aviv University, Tel Aviv 69978, Israel

Victor Chernomordik* and Amir Gandjbachkhe

National Institute of Child Health and Development, National Institutes of Health, Bethesda, Maryland 20892-5626

Received September 16, 2003

Fluorescent optical imaging of tumors deep within tissue depends on specific binding of antibodies to the tumors' surface markers. These fluorescent antibodies propagating in the vicinity of the tumor can be attached to and (or) diffused away from it. We illustrate application of a new tool, based on the random-walk theory in turbid media, for extracting the pharmacokinetics of these fluorescent antibodies by data deconvolution, excluding the effect of upper turbid tissue layers. © 2004 Optical Society of America

OCIS codes: 170.4580, 170.3660.

Tremendous advances in the molecular biology of disease processes and the development of specific fluorescently labeled cell markers as specific sources of optical contrast have opened the perspective of noninvasive quantification of disease processes. In small animal imaging it is desirable to be able to monitor the pharmacokinetics of these specific markers and their diffusion through tissue as a function of time, to identify the window of time in which only specific binding occurs. However, strong scattering of light dictates the use of photon migration theories for the quantification of pertinent parameters. Different groups of researchers have either developed or used optical contrast agents for imaging by reconstructing the concentration of fluorescent particles beneath the tissue.[1–5] The use of IR contrast agents to enhance imaging in phantom experiments has also been reported.[6] In previous stages of our work we were able to reconstruct the locations of tumors beneath the tissue surface[7] and quantify peak fluorescence intensity decay times as measured by spectrophotomers.[8] In this Letter we report on an original method of deconvolving the signal coming from deep structures and retrieve the true pharmacokinetics of tumor cells. Two pertinent parameters, i.e., temporal change in the peak intensities of the fluorescent signals and their full width at half-maximum, are used to study the dynamics of labeled antibodies.

In our animal experiments the tongues of Balb-C mice are injected with squamous carcinoma cells that are CD3 and CD19 positive. Fluorescein-isothiocyanate-conjugated antibodies to CD3 or CD19 are then injected into the tongue. First, the tongue is imaged after the fluorescent antibodies are injected at different time intervals to assess the pharmacokinetics of the fluorescent antibodies. In a separate experiment the same procedure is used, but the tongue is covered by an agarose slab with optical properties similar to those of the surrounding tissue. Details on tumor induction procedure can be found in Ref. 9, and quantities and application of the antibody-fluorophore conjugates protocol can be found in Ref. 7.

A series of surface fluorescence images were taken from each mouse as a function of time, from time of injection (every 2 min for the first 30 min and then every 5 min for 90 min; the total session time was 120 min). As an example, a recorded surface fluorescence image obtained from a 20-day-old tumor targeted with fluorescent antibodies, beneath a 1.95-mm slab of agarose is shown in Fig. 1.

Our method involves several steps. First, we use our random walk formulas for cw reflectance imaging of quasi-point fluorophores inside a turbid medium to retrieve the depth (more accurately, the centroid) of the fluorescent mass.[10,11] The corresponding expression is

$$\Gamma(\mathbf{r},\mathbf{r}_f) = \overline{A}[H(\alpha_-,\beta_-) - H(\alpha_-,\beta_+) - H(\alpha_+,\beta_-) + H(\alpha_+,\beta_+)]\exp\left(-\frac{\mu_{ae}}{\mu'_{se}}\right), \quad (1)$$

where

$$\alpha_\pm = \frac{3}{4}\left[\overline{x}_f^2 + \overline{y}_f^2 + \left(\overline{z}_f \pm \frac{\sqrt{2}}{\mu'_{si}}\right)^2\right]\mu_{si}'^2,$$

$$\beta_\pm = \frac{3}{4}\left[(\overline{x}_f - \overline{x})^2 + (\overline{y}_f - \overline{y})^2 + \left(\overline{z}_f + \frac{\sqrt{2}}{\mu'_{se}} \pm \frac{\sqrt{2}}{\mu'_{se}}\right)^2\right]\mu_{se}'^2,$$

$$H(\alpha,\beta) = \frac{1}{\sqrt{\alpha\beta}}\exp\left[-2\left(\sqrt{\alpha}\,\frac{\mu_{ai}}{\mu'_{si}} + \sqrt{\beta}\,\frac{\mu_{ae}}{\mu'_{se}}\right)\right].$$

Scaling factor $\overline{A}$ is neglected in further data analysis, since we are dealing only with normalized intensity

0146-9592/04/070742-03$15.00/0

distributions (it is determined by the fluorescence quantum efficiency Φ; the optical characteristics of the fluorescent agents, μ'_{sf} and μ'_{af}, as well as an effect of the probability multiple passage of the incident photons through the fluorescent site[12]). The origin of the coordinate system (0, 0, 0) is placed at the entry point of the incident photon, and the fluorophore and the detector are at $\mathbf{r}_f = (\overline{x}_f, \overline{y}_f, \overline{z}_f)$ and $\mathbf{r} = (\overline{x}, \overline{y}, \overline{z})$, respectively. The optical parameters in this equation, μ'_s and μ_a, are the transport-corrected scattering coefficient and the absorption coefficient of the background, respectively. Subscripts i and e stand for incident and emitted light, respectively. It should be noted that, for several fluorescent sites, the detected signal could be considered as a sum of signals from individual fluorophores. This method provides accurate reconstruction of the depth of the tumor beneath several agarose slabs with differing thicknesses at early stages of tumor development. At later stages of tumor development (when the size of the fluorophore becomes comparable with its depth), direct application of Eq. (1) for localization is not justified. However, if the centroid of the tumor is localized (e.g., estimated at early stages of the tumor growth),[7] then, to follow the pharmacokinetics of the injected fluorophore-antibody molecules at these later stages, one can use Eq. (1) as a point-spread function (PSF) for analysis of the experimental fluorescent images taken at subsequent times. In fact, the intensity distributions observed at the surface represent a convolution of these PSFs, $\Gamma(\mathbf{r}, \mathbf{r}_f)$, with the concentration distribution of the fluorescent molecules at the corresponding stage of tumor growth at time t, $N(\mathbf{r}_f, t)$:

$$I(\mathbf{r}, t) = \Gamma(\mathbf{r}, \mathbf{r}_f) \otimes N(\mathbf{r}_f, t)\,. \tag{2}$$

Thus, the true fluorophore concentration distribution, i.e., the expected intensity distribution when the tumor is superficial, can be obtained by deconvolution of the measured images from the effects of tissue scattering. We perform this deconvolution in the frequency domain, where convolution corresponds to the product of Fourier transforms of PSF $[\overline{\gamma}(\mathbf{x})]$ and the fluorophore's concentration profile $[\tilde{n}(\mathbf{x})]$. Thus,

$$N(\mathbf{r}_f, t) \propto \Phi^{-1}[i(\mathbf{x})/\gamma(\mathbf{x})]\,, \tag{3}$$

where $i(\mathbf{x})$ corresponds to the Fourier transform of the observed emitted intensity distribution and Φ^{-1} is the inverse Fourier transform.

Our analysis is two-dimensional deconvolution, which suggests that the centroid of the tumor is not migrating. The PSF given by Eq. (1) can be well approximated by a Lorentzian:

$$\Gamma(\mathbf{r}, \mathbf{r}_f) = \frac{A}{[b(z_f)^2 + (x - x_f)^2][b(z_f)^2 + (y - y_f)^2]} \tag{4}$$

(see, e.g., Fig. 2).

However, the observed one-dimensional intensity distributions of the scans passing through the point of maximum intensity of the emitted light proved to be close to Lorentzian as well, as shown in Fig. 3, in which we present an example of the observed one-dimensional intensity scans (the fluorophore depth is 1.95 mm):

$$I(\mathbf{r}, t) = \frac{A}{[\sigma_x(t)^2 + (x - x_m)^2][\sigma_y(t)^2 + (y - y_m)^2]}\,, \tag{5}$$

with effective widths $\sigma_x \approx \sigma_y = 3$–$5$ mm.

It follows from Eqs. (3)–(5) that an average concentration profile of the fluorescent agent is also close to Lorentzian, with effective widths $s_{x,y} = \sigma_{x,y} - b$, where b corresponds to the effective width of the PSF from Eq. (4).

In Fig. 4 we present an example of variation of the widths of the fluorescent intensity distributions, as a function of time after the injection (t = 10, 45, 70, 90, 120 min) for one series of measurements. As expected, the deconvolved values are much smaller than those expected without the presence of a turbid medium (at a fluorophore depth equal to 0). For comparison we also present in this figure an observed dependence of the surface intensity distribution width on time after injection t for zero fluorophore depth (different animal). One can see the

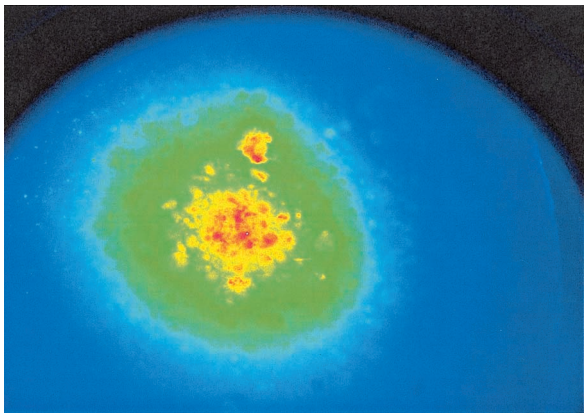

Fig. 1. Surface fluorescence image of a fluorophore in a 20-day-old tumor 1.95 mm beneath the surface 90 min after injection of fluoresceinated antibodies.

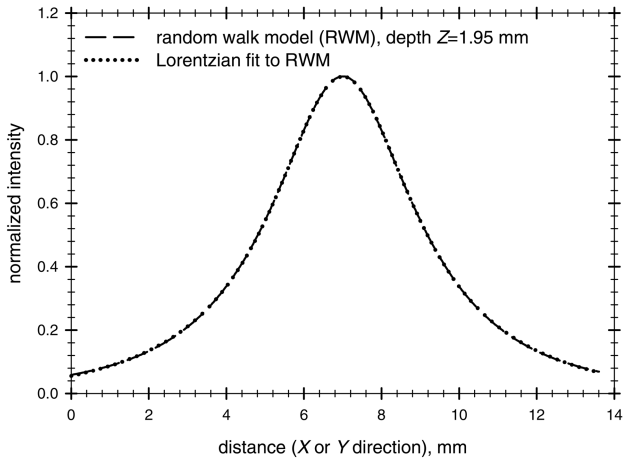

Fig. 2. Lorentzian fit to the random-walk model or 1.95-mm-deep fluorescence center.

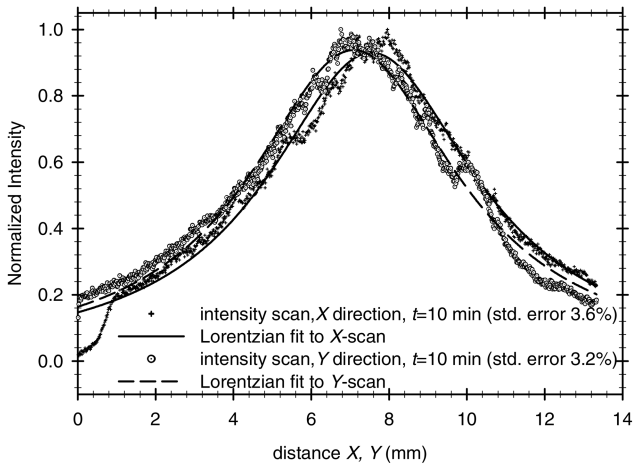

Fig. 3. Lorentzian fit to the scan through peak fluorescence data measured in the x and y directions.

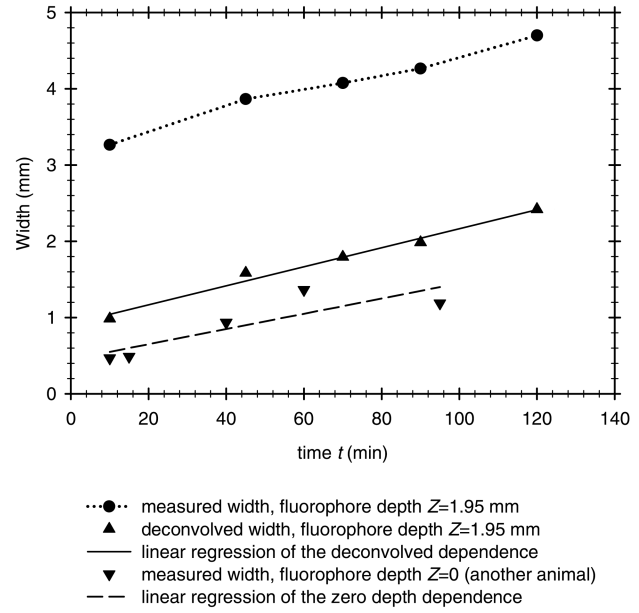

Fig. 4. Fluorescence signal width as a function of time.

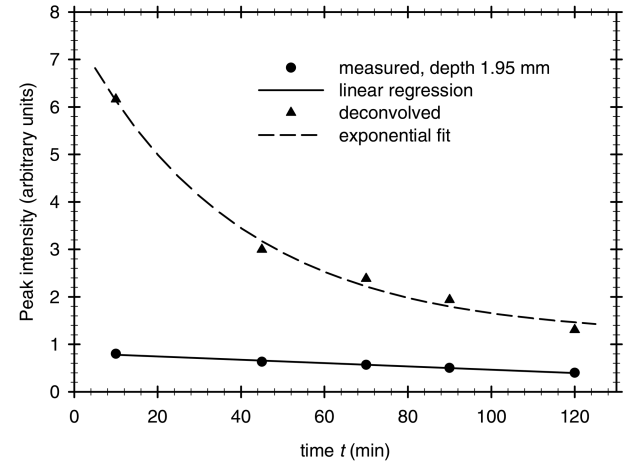

Fig. 5. Fluorescence peak intensities (measured and deconvolved) as functions of time after injection.

qualitative similarity between the surface distribution and reconstructed (deconvolved) dependence.

In Fig. 5 the fluorescence peak intensities (measured and deconvolved) are presented as functions of time after injection. Deconvolved peak intensities were estimated as inversely proportional to the squared width of the corresponding concentration profile (i.e., assuming that the total amount of the fluorophore inside the mouse tongue does not change during observations). As expected, these peak intensities decrease with time because of diffusion (washout) of the fluorescent particles. It is worth noting that, compared with the relatively slow decrease in intensity observed through the 1.95-mm layer of the turbid medium, the deconvolved peak values decrease much faster (exponentially), similarly to the experimental case of zero fluorophore depth (Fig. 5). It is obvious that the accuracy of our reconstruction procedure critically depends on the accuracy of the PSF used, i.e., the accuracy of the initial estimate of fluorophore depth $\overline{z}_f$. Fortunately, our model can provide good accuracy of depth $\overline{z}_f$ reconstruction (error $<10\%$) at the early stages of tumor development, as was demonstrated in Ref. 7.

In summary, the results of our experiments show that tissue scattering distorts the functional form of the pharmacokinetics. Using our model of diffuse fluorescent photon migration, we are able to deconvolve the signal coming from the deep structure and retrieve the true pharmacokinetics of the antibody fluorophore. These results show clearly that our mathematical model is able to quantify not only the three-dimensional localization of fluorescently labeled antibodies but also their clearance and diffusion through tissue.

I. Gannot's e-mail address is gannot@eng.tau.ac.il.
*These authors contributed equally to this work.

References

1. C. Bremer, V. Ntziachristos, and R. Weissleder, Eur. Radiol. **13,** 231 (2003).
2. J. E. Bugaj, S. Achilefu, R. B. Dorshow, and R. Rajagopalan, J. Biomed. Opt. **6,** 122 (2001).
3. X. Intes, J. Ripoll, Y. Chen, S. Nioka, A. G. Yodh, and B. Chance, Med. Phys. **30,** 1039 (2003).
4. J. S. Lewis, S. Achilefu, J. R. Garbow, R. Laforest, and M. J. Welch, Eur. J. Cancer **38,** 2173 (2002).
5. R. Weissleder and V. Ntziachristos, Nature Med. **9,** 123 (2003).
6. A. B. Thompson, D. J. Hawrysz, and E. M. Sevick-Muraca, Appl. Opt. **42,** 4125 (2003).
7. I. Gannot, A. Garashi, G. Gannot, V. Chernomordik, and A. H. Gandjbakhche, Appl. Opt. **42,** 3073 (2003).
8. I. Gannot, G. Gannot, A. Garashi, A. H. Gandjbakhche, A. Buchner, and Y. Keisari, J. Biomed. Opt. **7,** 14 (2002).
9. G. Gannot, I. Gannot, A. Buchner, H. Vered, and Y. Keisari, Br. J. Cancer **86,** 1444 (2002).
10. A. H. Gandjbakhche and I. Gannot, IEEE J. Sel. Top. Quantum Electron. **2,** 914 (1996).
11. A. H. Gandjbakhche, R. F. Bonner, R. Nossal, and G. H. Weiss, Appl. Opt. **36,** 4613 (1997).
12. A. H. Gandjbakhche and G. H. Weiss, in *Progress in Optics*, E. Wolf, ed. (Elsevier, Amsterdam, 1995), Vol. XXXIV, pp. 335–402.